ELSEVIER

Comput. Methods Appl. Mech. Engrg. 161 (1998) 229–243

Computer methods in applied mechanics and engineering

A unified finite element formulation for compressible and incompressible flows using augmented conservation variables

S. Mittal[a], T. Tezduyar[b,*]

[a]*Department of Aerospace Engineering, Indian Institute of Technology, Kanpur, UP 208 016, India*

[b]*Department of Aerospace Engineering and Mechanics, Army High Performance Computing Research Center, University of Minnesota, 1100 Washington Avenue South, Minneapolis, MN 55415, USA*

Received 6 November 1997

Abstract

A unified approach to computing compressible and incompressible flows is proposed. The governing equation for pressure is selected based on the local Mach number. In the incompressible limit the divergence-free constraint on velocity field determines the pressure, while it is the equation of state that governs the pressure solution for the compressible flows. Stabilized finite element formulations, based on the space–time and semi-discrete methods, with the 'augmented' conservation variables are employed. The 'augmented' conservation variables consist of the usual conservation variables and pressure as an additional variable. The formulation is applied to various test problems involving steady and unsteady flows over a large range of Mach and Reynolds numbers.

1. Introduction

Computational methods to solve flow problems fall mainly into two categories: (a) methods for compressible flows and (b) methods for incompressible flows. These two cases of methods are quite different from each other with respect to the choice of variables, issues related to numerical stability and choice of solvers. Various researchers in the past have proposed ideas for a unified approach to compressible and incompressible flows. Turkel [1] suggested a preconditioning method to accelerate the convergence to a steady state for both the compressible and incompressible flow equations. Hauke and Hughes [2] and Hauke [3] presented a finite element formulation for solving the compressible Navier–Stokes equations with different sets of variables. They also showed that in the context of primitive or entropy variables, the incompressible limit is well behaved and therefore, one formulation can be used for solving both compressible and incompressible flows. Weiss and Smith [4] proposed a preconditioning technique in conjunction with a dual time-step procedure to compute unsteady compressible and incompressible flows with density-based variables. Karimian and Schneider [5] presented a collocated pressure-based method that works in both compressible and incompressible regimes.

In this article we present an alternate, unified approach to computing compressible and incompressible flows using 'augmented' conservation variables formulation. Compressible flows have been computed by several researchers in the past with the conservation variables formulation [6–13]. It was shown by Hauke [3], that in the incompressible limit, the Euler Jacobians for the formulation employing conservation variables is not well behaved. In the incompressible limit, since density becomes constant, some of the coefficients must go to infinity to accommodate finite variations in pressure. It has also been shown by Panton [14] that in the

* Corresponding author.

0045-7825/98/$19.00
PII: S0045-7825(97)00318-6

incompressible limit, the state equation degenerates to a result according to which the density of a fluid particle is constant. This relation along with the mass balance equation leads to the divergence-free constraint on the velocity field that can be used to determine the pressure in incompressible flows. The formulation that we propose in this article is based on the philosophy that pressure is determined by the equation of state when the flow is compressible, whereas it is determined by the divergence-free constraint when the flow is incompressible. To this end we employ the 'augmented' conservation variables which consist of the usual conservation variables (density, momenta and energy) and pressure as an additional variable.

We begin by reviewing the governing equations for compressible and incompressible fluid flow in Section 2. The equations are cast in a non-dimensional form and a parameter z, based on the local Mach number, is introduced that governs the choice of equations for compressible and incompressible flows locally in the computational domain. The stabilized space–time variational formulation of these equations in terms of the augmented conservation variables is presented in Section 3. The SUPG (streamline-upwind/Petrov–Galerkin) stabilization technique [6,7,9,13,15,16] is employed to stabilize our computations against spurious numerical oscillations. In Section 4 we present some numerical results to test the performance of the proposed formulation. We begin with the computation of the shock-reflection problem that involves three flow regions separated by an oblique shock and its reflection from a wall. The exact solution for this problem is known and is compared with the computed solution. Next, supersonic flow past a cylinder at Mach 2 and Re 2000 is computed with the unified formulation and with the compressible flow formulation based on the equation of state. Finally, results are presented for unsteady flow past a cylinder at Re 100. These computations are carried out for different subsonic Mach numbers including the incompressible limit.

2. The governing equations

Let $\Omega_t \subset \mathbb{R}^{n_{sd}}$ and $(0, T)$ be the spatial and temporal domains, respectively, where n_{sd} is the number of space dimensions, and let Γ_t denote the boundary of Ω_t. The spatial and temporal coordinates are denoted by $\boldsymbol{x}$ and t. The Navier–Stokes equations governing the fluid flow, in conservation form, are

$$\frac{\partial \rho}{\partial t} + \nabla \cdot (\rho \boldsymbol{u}) = 0 \quad \text{on } \Omega_t \text{ for } (0, T), \tag{1}$$

$$\frac{\partial (\rho \boldsymbol{u})}{\partial t} + \nabla \cdot (\rho \boldsymbol{u}\boldsymbol{u}) + \nabla p - \nabla \cdot \boldsymbol{T} = \boldsymbol{0} \quad \text{on } \Omega_t \text{ for } (0, T), \tag{2}$$

$$\frac{\partial (\rho e)}{\partial t} + \nabla \cdot (\rho e \boldsymbol{u}) + \nabla \cdot (p \boldsymbol{u}) - \nabla \cdot (\boldsymbol{T}\boldsymbol{u}) + \nabla \cdot \boldsymbol{q} = 0 \quad \text{on } \Omega_t \text{ for } (0, T). \tag{3}$$

Here, ρ, $\boldsymbol{u}$, p, $\boldsymbol{T}$, e, and $\boldsymbol{q}$ are the density, velocity, pressure, viscous stress tensor, total energy per unit mass, and heat flux vector, respectively. The viscous stress tensor is defined as

$$\boldsymbol{T} = \mu((\nabla \boldsymbol{u}) + (\nabla \boldsymbol{u})^{\mathrm{T}}) + \lambda(\nabla \cdot \boldsymbol{u})\boldsymbol{I}. \tag{4}$$

where μ and λ are the viscosity coefficients. It is assumed that μ and λ are related by

$$\lambda = -\frac{2}{3}\mu. \tag{5}$$

Pressure is related to the other variables via the equation of state. For ideal gases, the equation of state assumes the special form

$$p = (\gamma - 1)\rho i, \tag{6}$$

where γ is the ratio of specific heats, and i is the internal energy per unit mass which is related to the total energy per unit mass and kinetic energy as

$$i = e - \frac{1}{2}\|\boldsymbol{u}\|^2. \tag{7}$$

The heat flux vector is defined as

$$\boldsymbol{q} = -\kappa \nabla \theta \,, \tag{8}$$

where κ is the heat conductivity and θ is the temperature. the temperature is related to the internal energy by the following relation:

$$\theta = \frac{i}{C_v}, \tag{9}$$

where C_v is the specific heat of the fluid at constant volume. For an ideal gas

$$C_v = \frac{R}{\gamma - 1}, \tag{10}$$

where R is the ideal gas constant. Prandtl number (P_r), assumed to be specified, relates the heat conductivity of the fluid to its viscosity according to the following relation:

$$\kappa = \frac{\mu C_p}{P_r}, \tag{11}$$

where C_p is the specific heat of the fluid at constant pressure. For an ideal gas

$$C_p = \frac{\gamma R}{\gamma - 1}. \tag{12}$$

In the limit of incompressible flows, i.e. when the Mach number approaches zero, the above-mentioned set of equations assume a new form. It can be shown [14], that the state equation along with the mass balance equation lead to the following relation:

$$\rho \nabla \cdot \boldsymbol{u} = 0. \tag{13}$$

Using the relation, Eqs. (1), (2) and (3) can be modified for incompressible flows as

$$\frac{\partial \rho}{\partial t} + \nabla \cdot (\rho \boldsymbol{u}) - \rho \nabla \cdot \boldsymbol{u} = 0 \quad \text{on } \Omega_t \text{ for } (0, T), \tag{14}$$

$$\frac{\partial (\rho \boldsymbol{u})}{\partial t} + \nabla \cdot (\rho \boldsymbol{u}\boldsymbol{u}) - \rho \boldsymbol{u} \nabla \cdot \boldsymbol{u} + \nabla p - \nabla \cdot \boldsymbol{T} = 0 \quad \text{on } \Omega_t \text{ for } (0, T), \tag{15}$$

$$\frac{\partial (\rho e)}{\partial t} + \nabla \cdot (\rho e \boldsymbol{u}) - \rho e \nabla \cdot \boldsymbol{u} + \nabla \cdot (p \boldsymbol{u}) - p \nabla \cdot \boldsymbol{u} - \nabla \cdot (\boldsymbol{T}\boldsymbol{u}) + \nabla \cdot \boldsymbol{q} = 0 \quad \text{on } \Omega_t \text{ for } (0, T). \tag{16}$$

In this situation, the viscous stress tensor, given by Eq. (4) can be rewritten as

$$\boldsymbol{T} = \mu((\nabla \boldsymbol{u}) + (\nabla \boldsymbol{u})^{\mathrm{T}}). \tag{17}$$

It is possible to combine the two sets of governing equations for the compressible and incompressible flows and express them in terms of non-dimensional variables. The non-dimensional variables that we choose are

$$\begin{aligned} \boldsymbol{x}^* &= \frac{\boldsymbol{x}}{L}, \qquad \boldsymbol{u}^* = \frac{\boldsymbol{u}}{U_\infty}, \qquad t^* = \frac{t U_\infty}{L}, \qquad \rho^* = \frac{\rho}{\rho_\infty}, \\ p^* &= \frac{p - p_\infty}{\rho_\infty U_\infty^2}, \qquad \theta^* = \frac{(\theta - \theta_\infty) C_p}{U_\infty^2}, \end{aligned} \tag{18}$$

where all the quantities with the subscript '∞' refer to the free-stream values of the flow variables. The governing equations in the non-dimensional variables that are valid over the entire range of compressible and incompressible flows are

$$\frac{\partial \rho^*}{\partial t^*} + \nabla^* \cdot (\rho^* \boldsymbol{u}^*) - (1 - z) \rho^* \nabla^* \cdot \boldsymbol{u}^* = 0 \quad \text{on } \Omega_t^* \text{ for } (0, T^*), \tag{19}$$

$$\frac{\partial (\rho^* \boldsymbol{u}^*)}{\partial t} + \nabla^* \cdot (\rho^* \boldsymbol{u}^* \boldsymbol{u}^*) - (1 - z) \rho^* \boldsymbol{u}^* \nabla^* \cdot \boldsymbol{u}^* + \nabla^* p^* - \nabla^* \cdot \boldsymbol{T}^* = 0 \quad \text{on } \Omega_t^* \text{ for } (0, T^*), \tag{20}$$

$$z\left[p^* + \frac{1}{\gamma M_\infty^2} - \frac{\rho^*}{\gamma M_\infty^2}\{1 + (\gamma - 1)M_\infty^2\theta^*\}\right] + (1 - z)[\rho^*\nabla^* \cdot \boldsymbol{u}^*] = 0 \quad \text{on } \Omega_t^* \text{ for } (0, T^*), \tag{21}$$

$$\frac{\partial(\rho^* e^*)}{\partial t^*} + \nabla^* \cdot \left(\rho^* e^* \boldsymbol{u}^* + p^* \boldsymbol{u}^* + \frac{z}{\gamma M_\infty^2}\boldsymbol{u}^*\right) - (1 - z)[(\rho^* e^* + p^*)\nabla^* \cdot \boldsymbol{u}^*] - \nabla^* \cdot (\boldsymbol{T}^* \boldsymbol{u}^*) + \nabla^* \cdot \boldsymbol{q}^* = 0 \quad \text{on } \Omega_t^* \text{ for } (0, T^*). \tag{22}$$

The Mach number (M) is defined as the ratio of the flow speed to the speed of sound; M_∞ refers to the free-stream Mach number. In the above equations $z(M) \in [0, 1]$ is a function of Mach number such that $z(0) = 0$ and $z(M \geq M_c) = 1$, where M_c is a 'cut-off' Mach number, decided a priori. All the results reported in this article are with $M_c = 0.3$ and with the following definition of z:

$$z = \begin{cases} \left(\dfrac{M}{M_c}\right)^4 & M \leq M_c \\ 1 & M > M_c \end{cases}. \tag{23}$$

The non-dimensional viscous stress tensor and heat flux vector are defined as

$$\boldsymbol{T}^* = \frac{1}{R_e}\left[(\nabla^* \boldsymbol{u}^*) + (\nabla^* \boldsymbol{u}^*)^{\mathrm{T}} - \frac{2}{3} z(\nabla^* \cdot \boldsymbol{u}^*)\boldsymbol{I}\right], \tag{24}$$

$$\boldsymbol{q}^* = -\frac{1}{R_e P_r}\nabla^* \theta^*. \tag{25}$$

Here, R_e is the Reynolds Number defined as

$$R_e = \frac{\rho_\infty U_\infty L}{\mu}. \tag{26}$$

In the rest of the article we will work with the non-dimensional variables only and therefore, the superscript '$*$' will be dropped. The governing equations (19)–(22) can be written in the augmented conservation variables

$$\boldsymbol{M}\frac{\partial \boldsymbol{U}}{\partial t} + \frac{\partial \boldsymbol{F}_i}{\partial x_i} - \frac{\partial \boldsymbol{E}_i}{\partial xi} + \boldsymbol{B}_i \frac{\partial \boldsymbol{U}}{\partial x_i} + \boldsymbol{S}\boldsymbol{U} = \boldsymbol{0} \quad \text{on } \Omega_t \text{ for } (0, T), \tag{27}$$

where $\boldsymbol{U} = (\rho, \rho u_1, \rho u_2, p, \rho e)$, is the vector of augmented conservation variables and $\boldsymbol{M}$ is a diagonal matrix defined as $\boldsymbol{M} = \mathrm{diag}(1, 1, 1, 0, 1)$. The various terms involving z and $(1 - z)$ in Eqs. (19)–(22) contribute to the terms involving $\boldsymbol{B}_i$ and $\boldsymbol{S}$ in Eq. (27). $\boldsymbol{F}_i$ and $\boldsymbol{E}_i$ are, respectively, the Euler and viscous flux vectors defined as

$$\boldsymbol{F}_i = \begin{pmatrix} u_i \rho \\ u_i \rho u_1 + \delta_{i1} p \\ u_i \rho u_2 + \delta_{i2} p \\ 0 \\ u_i(\rho e + p) \end{pmatrix}, \tag{28}$$

$$\boldsymbol{Ei} = \begin{pmatrix} 0 \\ \tau_{i1} \\ \tau_{i2} \\ 0 \\ -q_i + \tau_{ik} u_k \end{pmatrix}. \tag{29}$$

Here, u_i and q_i are the components of the velocity and heat flux vectors, respectively, and τ_{ik} are the components of the viscous stress tensor. In the quasi-linear form, Eq. (27) is written as

$$\boldsymbol{M}\frac{\partial \boldsymbol{U}}{\partial t} + (\boldsymbol{A}_i + \boldsymbol{B}_i)\frac{\partial \boldsymbol{U}}{\partial x_i} - \frac{\partial}{\partial x_i}\left(\boldsymbol{K}_{ij}\frac{\partial \boldsymbol{U}}{\partial x_j}\right) + \boldsymbol{S}\boldsymbol{U} = 0 \quad \text{on } \Omega_t \text{ for } (0, T), \tag{30}$$

where

$$\boldsymbol{A}_i = \frac{\partial \boldsymbol{F}_i}{\partial \boldsymbol{U}}, \tag{31}$$

is the Euler Jacobian Matrix, and $\boldsymbol{K}_{ij}$ is the diffusivity matrix satisfying

$$\boldsymbol{K}_{ij}\frac{\partial \boldsymbol{U}}{\partial x_j} = \boldsymbol{E}_i . \tag{32}$$

Corresponding to Eq. (30), appropriate boundary and initial conditions are chosen.

3. Finite element formulation

In order to construct the finite element function spaces for the space–time method, we partition the time interval $(0, T)$ into subintervals $I_n = (t_n, t_{n+1})$, where t_n and t_{n+1} belong to an ordered series of time levels $0 = t_0 < t_1 < \cdots < t_N = T$. Let $\Omega_n = \Omega_{t_n}$ and $\Gamma_n = \Gamma_{t_n}$. We define the space–time slab Q_n as the domain enclosed by the surfaces Ω_n, Ω_{n+1}, and P_n, where P_n is the surface described by the boundary Γ_t as t traverses I_n. The surface P_n is decomposed into $(P_n)_g$ and $(P_n)_h$ with respect to the type of boundary condition (Dirichlet or Neumann) being imposed. For each space–time slab we define the corresponding finite element function spaces $\mathcal{S}^h$ and $\mathcal{V}^h$. Over the element domain, this space is formed by using first-order polynomials in space and time. Globally, the interpolation functions are continuous in space but discontinuous in time.

The stabilized space–time formulation is written as follows: given $(\boldsymbol{U}^h)_n^-$, find $\boldsymbol{U}^h \in \mathcal{S}^h$ such that $\forall\, \boldsymbol{W}^h \in \mathcal{V}^h$,

$$\begin{aligned}
&\int_{Q_n} \boldsymbol{W}^h \cdot \boldsymbol{M}^h \frac{\partial \boldsymbol{U}^h}{\partial t}\,\mathrm{d}Q + \int_{Q_n} \left(\frac{\partial \boldsymbol{W}^h}{\partial x_i}\right)\cdot(-\boldsymbol{F}_i^h + \boldsymbol{E}_i^h)\,\mathrm{d}Q + \int_{Q_n} \boldsymbol{W}^h \cdot \left(\boldsymbol{B}_i^h \frac{\partial \boldsymbol{U}^h}{\partial x_i} + \boldsymbol{S}^h \boldsymbol{U}^h\right)\mathrm{d}Q \\
&\quad + \sum_{e=1}^{n_{\mathrm{el}}} \int_{Q_n^e} \boldsymbol{\tau}(\hat{\boldsymbol{A}}_k^h)^T \left(\frac{\partial \boldsymbol{W}^h}{\partial x_k}\right)\cdot\left[\boldsymbol{M}^h \frac{\partial \boldsymbol{U}^h}{\partial t} + (\boldsymbol{A}_i^h + \boldsymbol{B}_i^h)\frac{\partial \boldsymbol{U}^h}{\partial x_i} - \frac{\partial}{\partial x_i}\left(\boldsymbol{K}_{ij}^h \frac{\partial \boldsymbol{U}^h}{\partial x_j}\right) + \boldsymbol{S}^h \boldsymbol{U}^h\right]\mathrm{d}Q \\
&\quad + \sum_{e=1}^{n_{\mathrm{el}}} \int_{Q_n^e} \boldsymbol{\beta}\left(\frac{\partial \boldsymbol{W}^h}{\partial x_i}\right)\cdot\left[(z\boldsymbol{M}^h + (1-z)\boldsymbol{N}^h)\frac{\partial \boldsymbol{U}^h}{\partial x_i}\right]\mathrm{d}Q + \int_{\Omega_n} (\boldsymbol{W}^h)_n^+ \cdot \boldsymbol{M}^h((\boldsymbol{U}^h)_n^+ - (\boldsymbol{U}^h)_n^-)\,\mathrm{d}\Omega \\
&\quad = \int_{(P_n)_h} \boldsymbol{W}^h \cdot \boldsymbol{h}^h\,\mathrm{d}P .
\end{aligned} \tag{33}$$

Here, $\boldsymbol{h}^h$ represents the Neumann boundary condition imposed and $(P_n)_h$ is the part of the slab boundary with such conditions. the solution to (33) is obtained sequentially for all space–time slabs $Q_0, Q_1, Q_2, \ldots, Q_{N-1}$ and the computations start with

$$(\boldsymbol{U}^h)_0^- = \boldsymbol{U}_0 , \tag{34}$$

where $\boldsymbol{U}_0$ is the specified initial condition.

REMARKS

(1) In the variational formulation given by Eq. (33), the first three integrals and the right-hand side constitute the Galerkin formulation of the problem. Both the Euler and viscous flux terms are integrated by parts. This form of the variational formulation ensures that, in the presence of shocks, the method gives right jump conditions and shock location. The Neumann boundary condition at the outflow boundary involves the normal components of the stress vector and momentum flux. In the limit of incompressible flows (where the pressure is specified only upto a constant and one needs to define a datum pressure) this fixes the pressure at the boundary. To compute flows that involve free surfaces the weak form given by Eq. (33) has to be modified by carrying out the integration-by-part of the time-dependent term.

(2) The first series of element-level integrals in Eq. (33) are added to the variational formulation to stabilize the computations against numerical instabilities. In the advection-dominated range, these terms prevent the node-to-node oscillations of the flow variables. In the limit of incompressible flows, the inclusion of

these terms allows one to employ equal-order-interpolation for velocity and pressure. The choice of stabilization coefficient τ is quite different for compressible and incompressible flows. In the context of a unified formulation, one would like to design the stabilization coefficient τ such that it reduces to the appropriate definitions in the two limits. The second series of element level integrals in Eq. (33) are the shock capturing terms that stabilize the computations in the presence of sharp gradients. The coefficient of shock-capturing operator, β is same as defined in [13]. The stabilization coefficient τ is defined as

$$\tau = \max[\mathbf{0}, \tau_a - \tau_\beta], \tag{35}$$

where τ_a is a diagonal matrix defined as $\tau_a = \mathrm{diag}(\tau_1, \tau_1, \tau_1, \tau_2, \tau_1)$,

$$\tau_1 = \left(\left(\frac{2(c\hat{z} + \|\boldsymbol{u}\|)}{h}\right)^2 + \left(\frac{12\nu}{h^2}\right)^2\right)^{-1/2}, \tag{36}$$

$$\tau_2 = \frac{h}{2}\|\boldsymbol{u}^h\|\lambda, \tag{37}$$

$$\lambda = \begin{cases} \left(\dfrac{R_{eu}}{3}\right) & R_{eu} \leq 3 \\ 1 & R_{eu} > 3 \end{cases}. \tag{38}$$

In the above equations R_{eu} is the cell Reynolds number, c is the wave speed, $\|\boldsymbol{u}^h\|$ is the flow speed, and h is the element length. $\hat{z}(M) \in [0, 1]$ is a function of Mach number such that $\hat{z}(0) = 0$ and $\hat{z}(M \geq \hat{M}_c) = 1$. All the results reported in this article are with the following definition of $\hat{z}$:

$$\hat{z} = \begin{cases} \left(\dfrac{M}{\hat{M}_c}\right)^2 & M \leq \hat{M}_c \\ 1 & M > \hat{M}_c \end{cases}, \tag{39}$$

where $\hat{M}_c = 0.1$. Matrix τ_β is subtracted from τ_a to account for the shock-capturing term as shown in Eq. (35). It is defined as

$$\tau_\beta = \frac{\hat{z}\beta}{2(c + \|\boldsymbol{u}\|)^2}\boldsymbol{M}. \tag{40}$$

Consider the computation of compressible flow past a solid body using the unified formulation as in Eq. (33). In the regions where the mach number is low, for example in the boundary layer, the flow is almost incompressible and density assumes, approximately, the free-stream value. Under these conditions the continuity equation, Eq. (19), behaves like an advection equation for density. Farther away from the boundary layer, the flow is in the compressible regime and the density variations are quite significant. The term in Eq. (33) that involves $\boldsymbol{N}^h$ provides numerical stability to the density field in the region where the above-mentioned transition takes place. This term is not needed in the formulation if one is seeking solutions governed by either the compressible or the incompressible flow equations only. The matrix $\boldsymbol{N}^h$ is a diagonal matrix defined as $\boldsymbol{N}^h = \mathrm{diag}(1, 0, 0, 0, 0)$.

In the stabilizing terms in Eq. (33), components of the $\hat{\boldsymbol{A}}_k^h$ matrix are defined as

$$[\hat{\boldsymbol{A}}_k^h]_{i,j} = [\boldsymbol{A}_k^h]_{i,j} + z\delta_{i,k+1}\delta_{j,5}C, \tag{41}$$

where C is a constant. This term provides stability to the computations for compressible flows. Notice that such a term is not explicitly added to the formulation in terms of the conservation variables; a similar term is already present in the definition of $\boldsymbol{A}_k^h$. In the case of augmented conservation variables such a term is not present in the original definition of $\boldsymbol{A}_k^h$. It has been our experience, with augmented conservation variables formulation, that in the absence of this term the velocity field develops oscillations that grow with time. In our computations we choose $C = 2$.

(3) The sixth integral enforces weak continuity of the velocity field across the space–time slabs.
(4) If one is interested in strictly incompressible flows, Eq. (33) can still be used. However, to reduce the computational cost, one can prescribe the density field in the entire domain and therefore, not solve for it. Additionally, if one is not interested in the temperature field, one can drop the energy equation too. This is possible because in the incompressible limit, the energy equation is decoupled from the rest of the flow equations.
(5) The variational formulation in terms of the augmented conservation variables has an advantage that any change in the equation of state can be incorporated in the implementation with very little effort. For example, to include the real gas effects in the formulation, one needs to modify the state equation only. However, the implementation is not so straightforward if one uses the conservation variables.
(6) We also implemented this unified approach in the context of a semi-discrete formulation. In the incompressible limit, Eq. (21) reduces to the divergence free condition on the velocity field. It behaves like a constraint equation and one looks for a pressure field such that the velocity field satisfies the divergence free condition at each time level. In an implementation for time-accurate computation of incompressible flows, the divergence free equation and the pressure terms are evaluated at the $n+1$ time level while the rest of the terms are evaluated at $n+1/2$ time level. This ensures that the velocity field at each time level is divergence free. On the other hand, if the divergence free equation is evaluated at the $n+1/2$ time level, the velocity field computed at later times may not be divergence free and one cannot ensure the stability of computations. Therefore, in the semi-discrete implementation of the unified formulation for time-accurate computations, the pressure and the terms involving divergence of velocity are evaluated at $n+1$ time level while the other terms are evaluated at $n+1/2$ time level. We have computed unsteady solutions using, both, the space–time and semi-discrete implementations of our formulation. The results obtained from the two implementations are almost indistinguishable. In this article, therefore, we report the results only from the space–time implementation. It must be pointed out that the computations with the space–time method are substantially more expensive than the ones with the semi-discrete method. However, the space–time method allows one to compute flows involving moving boundaries and interfaces.

4. Numerical examples

Most of the computations reported in this article were carried out on the Digital 3000/300 AXP work-station at IIT Kanpur. Some were computed on the CRAY C90 at Networking Computing Services in Minneapolis, Minnesota. For the space–time implementations, the finite-element basis functions are bilinear-in-space and linear-in-time, and $2\times2\times2$ Gaussian quadrature is employed for numerical integration. The calculations with the semi-discrete implementation, based on bilinear finite-element basis functions, give almost indistinguishable results as the ones from the space–time method. In this article, only the results computed with the space–time method are shown. The nonlinear equation systems resulting from the finite-element discretization of the flow equations are solved using the Generalized Minimal RESidual (GMRES) technique [17] in conjunction with diagonal and block-diagonal preconditioners.

4.1. Shock-reflection problem

This two-dimensional, inviscid, steady problem involves three flow regions separated by an oblique shock and its reflection from a wall as shown in Fig. 1.

It is a standard benchmark problem and for more details the interested reader is referred to the work by Le Beau and Tezduyar [9] and Shakib [18]. The motivation for this computation is to establish confidence in our formulation and its implementation for computing flows involving shocks. The computational domain is a rectangular region of dimensions 4.1 in the x direction and 1.0 in the y direction. The mesh consists of 60×20 rectangular elements. At the left boundary, flow data corresponding to Mach 2.9 is prescribed:

$$\text{Region 1} \quad \begin{cases} M = 2.9 \\ \rho = 1 \\ u_1 = 1 \\ u_2 = 0 \\ \theta = 0 \end{cases} . \tag{42}$$

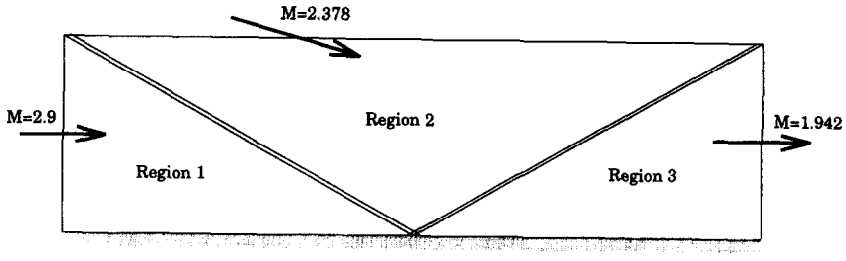

Fig. 1. Shock-reflection problem: problem description.

At the top boundary, the flow conditions that are specified correspond to Mach 2.3781 and an incident shock angle of 29°:

$$\text{Region 2} \quad \begin{cases} M = 2.3781 \\ \rho = 1.7 \\ u_1 = 0.9033 \\ u_2 = -0.1746 \\ \theta = 0.07685 \end{cases} . \tag{43}$$

At the lower boundary, the component of velocity normal to the wall is assigned a zero value. The computations begin with a uniform Mach 2.9 flow in the domain and continue till the steady-state norm drops below a certain

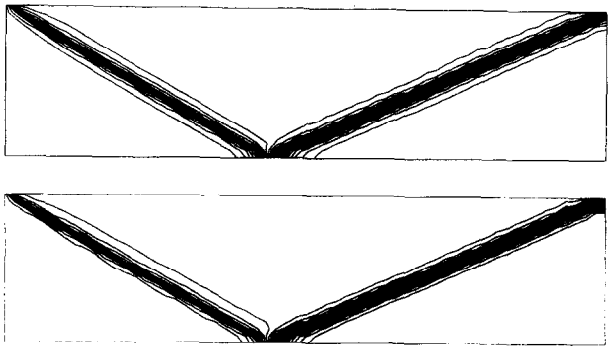

Fig. 2. Shock-reflection problem: density and pressure fields for the steady-state solution.

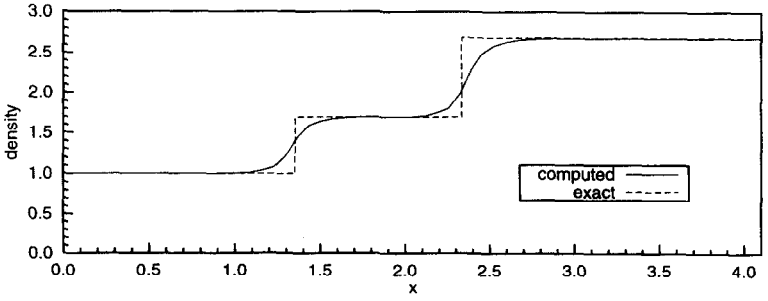

Fig. 3. Shock-reflection problem: density for the computed and exact solutions at $y = 0.25$.

value. It should be pointed out that in this problem, the local Mach number in the entire domain is always greater than the 'cut-off' Mach number defined in Eq. (23) and, therefore, $z = 1$ everywhere. This implies that the pressure is determined by the equation of state for perfect gas everywhere in the domain.

Fig. 2 shows the density and pressure fields in the domain for the steady-state solution. Compared in Fig. 3 are the density fields for the computed and exact solutions at $y = 0.25$. Our results compare quite well with those reported by other researchers using alternate formulations [9,18].

4.2. Supersonic flow past a cylinder

Mach 2 flow past a circular cylinder is computed for two cases. In the first case the original compressible flow equations are employed by setting $z = 1$ in Eqs. (19)–(22), i.e. the pressure is determined by the equation of state for a perfect gas. The second case is computed with the unified formulation where z is defined by Eq. (23). The mesh employed, consists of 5120 quadrilateral elements and 5264 nodes. The Reynolds number based on the diameter of the cylinder and the free-stream values of the velocity and kinematic viscosity is 2000, and the Prandtl Number is 0.72. The cylinder wall is assumed to be adiabatic and the no-slip condition is specified for the velocity on the surface of the cylinder. All the variables are specified at the upstream boundary. At the upper and lower boundaries, normal components of the velocity and heat flux are set to zero together with the tangential component of the stress vector. At the downstream boundary, we specify a Neumann-type boundary condition for the velocity and energy that is consistent with the variational formulation given by Eq. (33). The computations are initiated with free-stream conditions in the entire domain and continue till the steady-state norm of the solution falls below a certain desired value. Shown in Fig. 4 are the density, temperature and pressure fields for the steady-state solution computed and the augmented conservation values formulation with

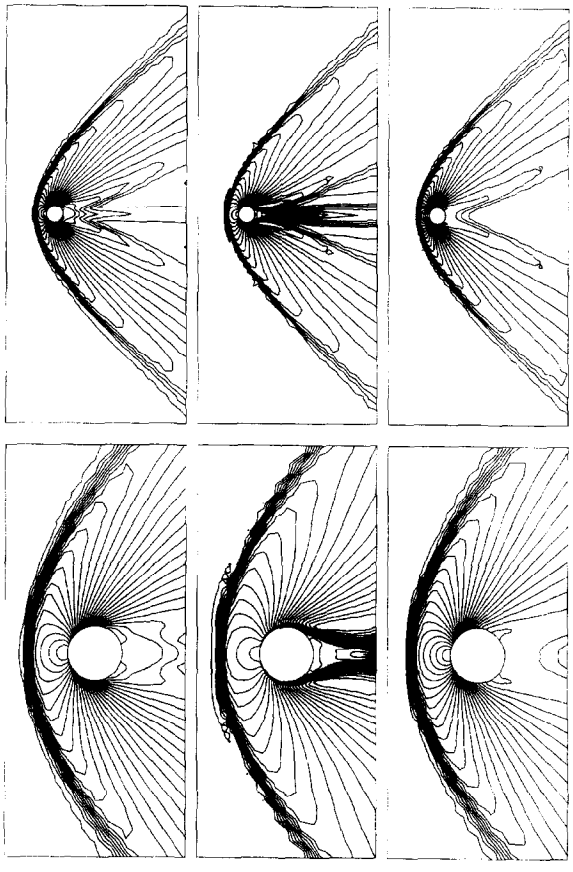

Fig. 4. Mach = 2, Re = 2000 flow past a cylinder computed with $z = 1$: density, temperature and pressure fields (and their close-ups in the lower row) for the steady-state solution.

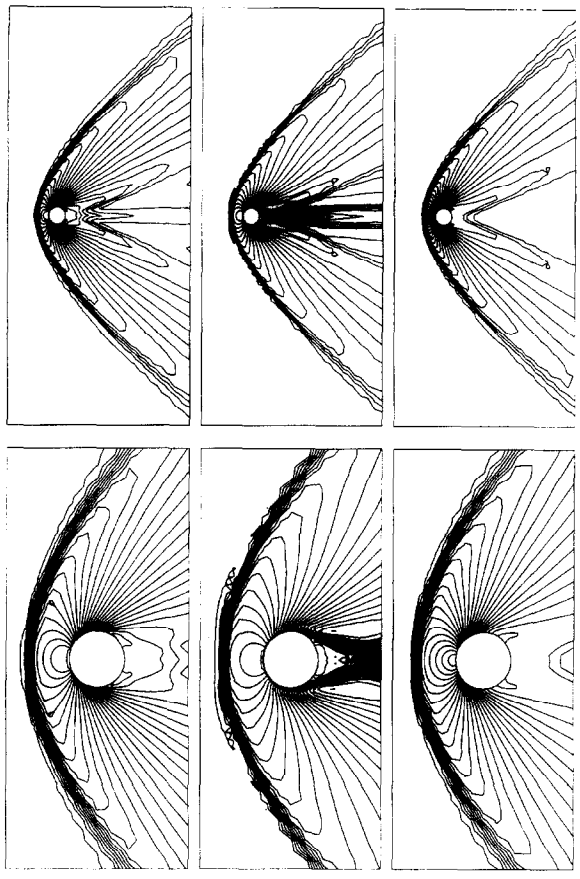

Fig. 5. Mach = 2, Re = 2000 flow past a cylinder computed with z defined by Eq. (23): density, temperature and pressure fields (and their close-ups in the lower row) for the steady-state solution.

$z = 1$. One can observe a strong bow shock upstream of the cylinder and a weak tail shock in the wake. The shock stand-off distance compares quite well with experimental observations [19]. It can also be observed that the shock has been captured quite well within two to three elements. Solution to the same problem has been computed by the conservation variables formulation on a much finer mesh with 16 000 elements and reported in [13]. On comparing the two solutions we observe that the conservation variables and the agumented conservation variables formulations lead to quite comparable results.

Fig. 5 shows the density, temperature and pressure fields for the steady-state solution computed with the unified formulation with z defined by Eq. (23). On comparing Figs. 5 and 4 we observe that they are quite similar except that the density and the temperature fields exhibit some differences close to the cylinder wall. In the case of unified formulation, with z defined by Eq. (23), the divergence-free constraint kicks-in very close to the wall of cylinder where the Mach number is nearly zero. In this region, the mass balance equation (19) behaves like an advection equation for density. As a result one observes from the contour plots, very close to the wall of the cylinder, that the flow attempts to advect the density from the upstream to downstream locations. This is certainly not the case in Fig. 5 where the pressure is determined by the state equation for a perfect gas and not by the divergence free constraint. It is quite interesting to note that the pressure fields computed by the two formulations are almost identical. The drag coefficient computed by both the formulations is 1.48.

These test problems demonstrate that the unified compressible–incompressible formulation results in correct shock location and strength for both viscous and inviscid flows.

4.3. Subsonic flow past a cylinder

The main motivation to develop the unified compressible–incompressible formulation is to improve the performance of compressible flow algorithm at low Mach numbers. In this section we present our solutions for

flow past a circular cylinder at Re 100 and low Mach numbers. The Prandtl Number is 0.72. The cylinder resides in a rectangular computational domain whose upstream and downstream boundaries are located at 15 and 35 cylinder radii, respectively, from the cylinder's center. The upper and lower boundaries are placed at 16 radii from the center of the cylinder. The finite element mesh consists of 4688 quadrilateral space–time elements and 4826 nodes. At each time step, 47 412 nonlinear equations are solved iteratively to compute the flow field. The cylinder surface is assumed to be adiabatic and the no slip condition is specified for the velocity on the cylinder wall. At the upstream boundary, density, velocity and temperature are assigned to their free-stream values. At the downstream boundary, we specify a Neumann-type boundary condition for the velocity and energy that is consistent with the variational formulation given by Eq. (33). At the upper and lower computational boundaries, normal components of the velocity and heat flux are set to zero together with the tangential component of the stress vector. We first present our results for Mach 0.2 flow computed with $z = 1$. Fig. 6 shows the vorticity, pressure and temperature fields corresponding to the peak value of lift coefficient. Fig. 7 shows the time histories of the lift and drag coefficients for that part of the simulation when the periodic solution is achieved. The Strouhal number corresponding to the variation of lift coefficient for this case is 0.164. Figs. 8 and 9 show the solution for Mach 0.2 flow computed with the unified formulation with z defined by Eq. (23). The Strouhal number corresponding to the variation of lift coefficient for this case is 0.169. As expected, the two solutions are quite similar. On comparing Figs. 6 and 8 we observe that there are some differences in the temperature fields of the two cases. As has been explained in the previous section, in the case of unified formulation, the flow very close to the wall is modeled by incompressible flow equations and therefore, the temperature changes take place only because of viscous effects. On the other hand, in the case of computations with $z = 1$, density, temperature and pressure changes take place in accordance with the equation of state for perfect gas. Therefore, the contribution to temperature changes come from, both, the viscous and compressible effects.

The formulation based purely on the compressible flow equations, i.e. with $z = 1$, fails to yield an acceptable unsteady solution at Mach 0.05 with the present mesh. However, if the mesh is refined it is possible to compute

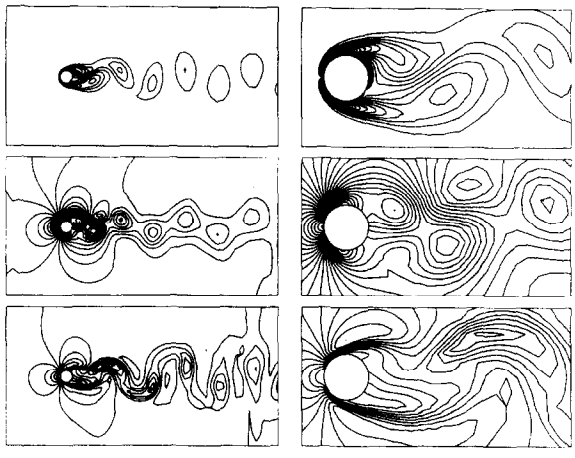

Fig. 6. Mach = 2, Re = 100 flow past a cylinder computed with $z = 1$: vorticity, pressure and temperature fields (and their close-ups on the right) at the peak value of the lift coefficient.

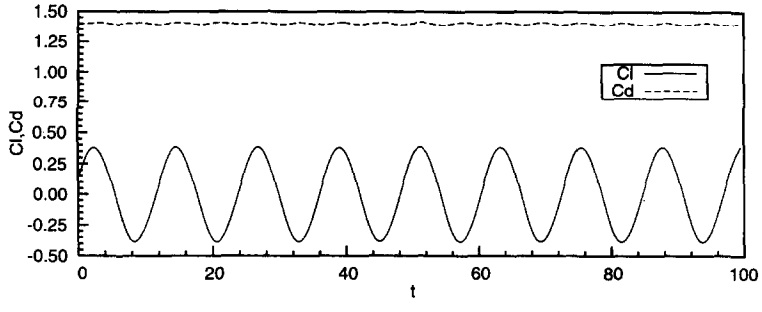

Fig. 7. Mach = 0.2, Re = 100 flow past a cylinder computed with $z = 1$: time histories of the lift and drag coefficients.

the unsteady flow at Mach 0.05. It has been our experience that the low Mach number flows are very sensitive to the spatial refinement. For a given mesh there exists a certain Mach number below which the compressible flow formulation breaks down. On the other hand, with the unified compressible–incompressible flow formulation, one is able to compute flows at any Mach number. Figs. 10 and 11 show the solution for unsteady flow past a cylinder at Mach 0.05 computed with z defined by Eq. (23). The Strouhal number corresponding to the variation

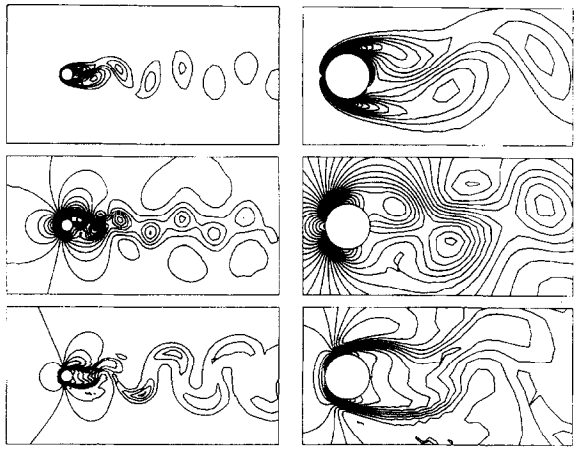

Fig. 8. Mach = 2, Re = 100 flow past a cylinder computed with z defined by Eq. (23): vorticity, pressure and temperature fields (and their close-ups on the right) at the peak value of the lift coefficient.

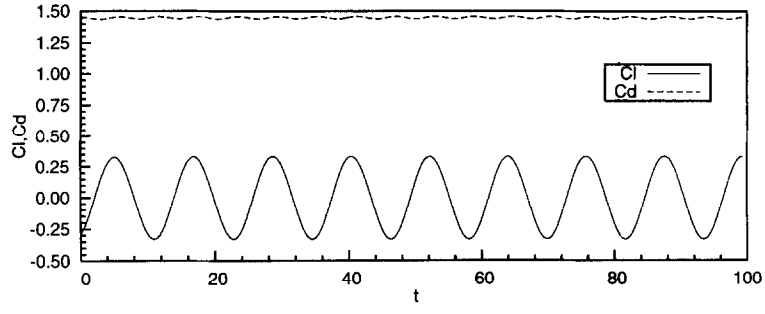

Fig. 9. Mach = 0.2, Re = 100 flow past a cylinder computed with z defined by Eq. (23): time histories of the lift and drag coefficients.

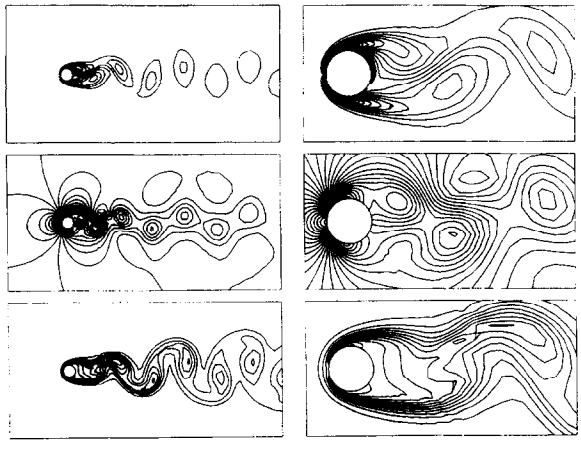

Fig. 10. Mach = 0.05, Re = 100 flow past a cylinder computed with z defined by Eq. (23): vorticity, pressure and temperature fields (and their close-ups on the right) at the peak value of the lift coefficient.

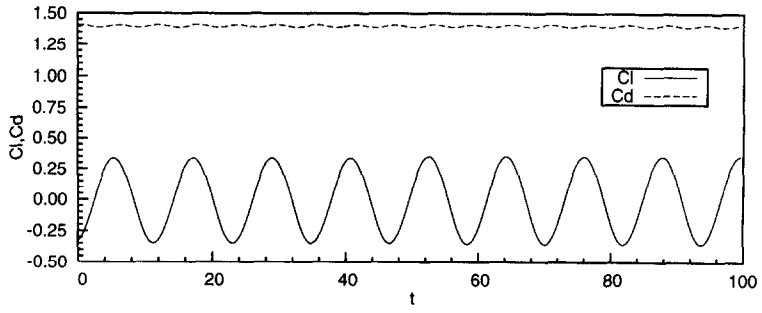

Fig. 11. Mach = 0.05, Re = 100 flow past a cylinder computed with z defined by Eq. (23): time histories of the lift and drag coefficients.

of lift coefficient for this case is 0.170. We observe that the solutions at Mach 0.05 and Mach 0.2 are quite similar except for certain differences in the temperature fields that are due to the compressibility effects. The demonstrate the robustness of the unified formulation we compute the unsteady flow past a cylinder at Mach 0.001 and in the incompressible limit. The solution at Mach 0.001 is shown in Figs. 12 and 13 while the one in the incompressible limit is shown in Figs. 14 and 15. The incompressible flow case is computed by setting $z = 0$. The Strouhal number for vortex shedding in both the cases is 0.170. We observe that the solutions for Mach numbers 0.05, 0.001 and in the incompressible limit are almost indistinguishable and agree quite well with results from alternate formulations for incompressible flows [20].

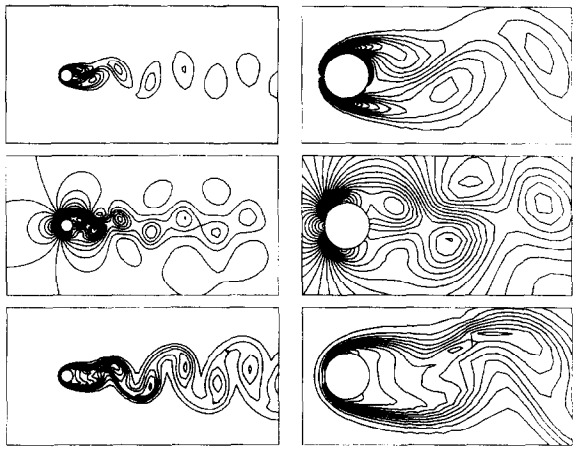

Fig. 12. Mach = 0.001, Re = 100 flow past a cylinder computed with z defined by Eq. (23): vorticity, pressure and temperature fields (and their close-ups on the right) at the peak value of the lift coefficient.

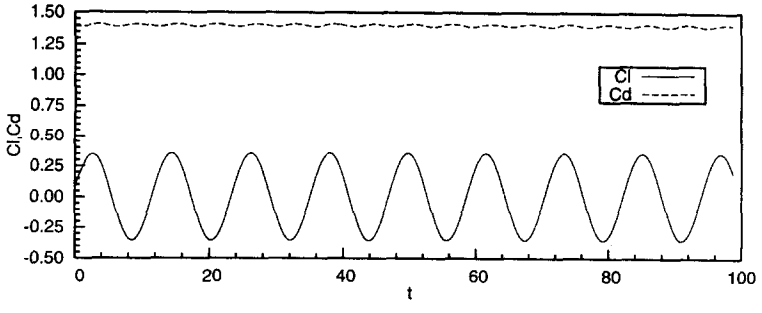

Fig. 13. Mach = 0.001, Re = 100 flow past a cylinder computed with z defined by Eq. (23): time histories of the lift and drag coefficients.

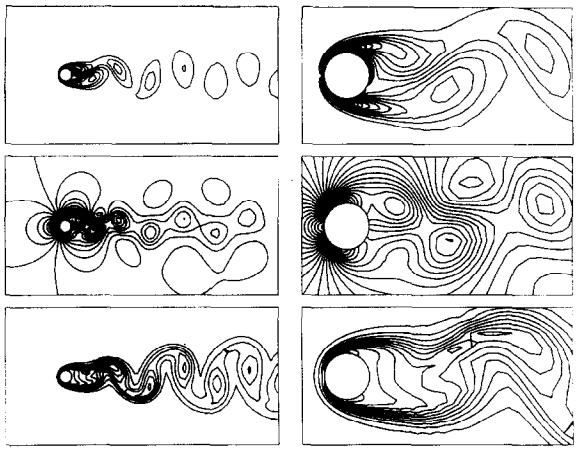

Fig. 14. Incompressible, Re = 100 flow past a cylinder computed with $z = 0$: vorticity, pressure and temperature fields (and their close-ups on the right) at the peak value of the lift coefficient.

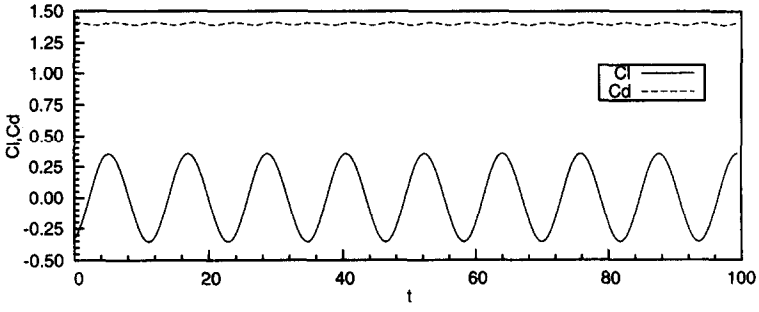

Fig. 15. Incompressible, Re = 100 flow past a cylinder computed with $z = 0$: time histories of the lift and drag coefficients.

5. Conclusions

A unified formulation for compressible and incompressible flows in terms of the augmented conservation variables has been proposed. In case of compressible flows the equation of state determines the pressure whereas it is the divergence-free constraint on velocity field that sets the pressure for incompressible flows. The appropriate governing equations are chosen locally based on the local Mach number. The formulation was successfully applied to various numerical tests involving steady and unsteady flows over a range of Mach and Reynolds numbers.

Acknowledgement

This work was sponsored by ARPA and by the Army High Performance Computing Research Center under the auspices of the Department of the Army, Army Research Laboratory cooperative agreement number DAAH04-95-2-0003/contract number DAHH04-95-0008. The content does not necessarily reflect the position or the policy of the government, and no official endorsement should be inferred. The CRAY time was provided, in part, by the University of Minnesota Supercomputer Institute.

References

[1] E. Turkel, Review of preconditioning methods for fluid dynamics, Technical Report 92-47, Institute for Computer Applications in Science and Engineering, NASA Langley Research Center, September 1992.

[2] G. Hauke and T.J.R. Hughes, A unified approach to compressible and incompressible flows, Comput. Methods Appl. Mech. Engrg. 113 (1994) 389–395.
[3] G. Hauke, A unified approach to compressible and incompressible flows and a new entropy-consistent formulation of the K-epsilon model, Ph.D. Thesis, Department of Mechanical Engineering, Stanford University, 1995.
[4] J.M. Weiss and W.A. Smith, Preconditioning applied to variable and constant density flows, AIAA J. 33(11) (1995) 2050–2057.
[5] S.M.H. Karimian and G.E. Schneider, Pressure-based control-volume finite element method for flow at all speeds, AIAA J. 33(9) (1995) 1611–1618.
[6] T.E. Tezduyar and T.J.R. Hughes, Development of time-accurate finite element techniques for first-order hyperbolic systems with particular emphasis on the compressible Euler equations, Report prepared under NASA-Ames University Consortium Interchange, No. NCA2-OR745-104, 1982.
[7] T.E. Tezduyar and T.J.R. Hughes, Finite element formulations for convection dominated flows with particular emphasis on the compressible Euler equations, in: Proc. AIAA 21st Aerospace Sciences Meeting, AIAA Paper 83-0125, Reno, Nevada, 1983.
[8] G.J. Le Beau, The finite element computation of compressible flows, Master's Thesis, Aerospace Engineering, University of Minnesota, 1990.
[9] G.J. Le Beau and T.E. Tezduyar, Finite element computation of compressible flows with the SUPG formulation, in: M.N. Dhaubhadel, M.S. Engelman and J.N. Reddy, eds., Advances in Finite Element Analysis in Fluid Dynamics, FED-Vol. 123 (ASME, New York, 1991) 21–27.
[10] G.J. Le Beau, S.E. Ray, S.K. Aliabadi and T.E. Tezduyar, SUPG finite element computation of compressible flows with the entropy and conservation variables formulations, Comput. Methods Appl. Mech. Engrg., 104 (1993) 27–42.
[11] S.K. Aliabadi and T.E. Tezduyar, Space–time finite element computation of compressible flows involving moving boundaries and interfaces, Comput. Methods Appl. Mech. Engrg. 107(1–2) (1993) 209–224.
[12] S.K. Aliabadi, S.E. Ray and T.E. Tezduyar, SUPG finite element computation of compressible flows with the entropy and conservation variables formulations, Comput. Mech. 11 (1993) 300–312.
[13] S. Mittal, Finite element computation of unsteady viscous compressible flows, Comput. Methods Appl. Mech. Engrg. (1997), to appear.
[14] R.L. Panton, Incompressible Flows (John Wiley and Sons, New York, 1984).
[15] T.J.R. Hughes and A.N. Brooks, A multi-dimensional upwind scheme with no crosswind diffusion, in: T.J.R. Hughes, ed., Finite Element Methods for Convection Dominated Flows, AMD-Vol. 34 (ASME, New York, 1979) 19–35.
[16] T.J.R. Hughes and T.E. Tezduyar, Finite element methods for first-order hyperbolic systems with particular emphasis on the compressible Euler equations, Comput. Methods Appl. Mech. Engrg. 45 (1984) 217–284.
[17] Y. Saad and M. Schultz, GMRES: A generalized minimal residual algorithm for solving nonsymmetric linear systems, SIAM J. Scient. Statist. Comput. 7 (1986) 856–869.
[18] F. Shakib, Finite element analysis of the compressible Euler and Navier–Stokes equations, Ph.D. Thesis, Department of Mechanical Engineering, Stanford University, 1988.
[19] H.W. Liepmann and A. Roshko, Elements of Gas Dynamics (John Wiley and Sons, Inc., New York, 1957).
[20] M. Behr, D. Hastreiter, S. Mittal and T.E. Tezduyar, Incompressible flow past a circular cylinder: Dependence of the computed flow field on the location of the lateral boundaries, Comput. Methods Appl. Mech. Engrg. 123 (1995) 309–316.